the evapotranspiration from an extensive surface of green grass of uniform height, actively growing, well-watered, and completely shading the ground" (Allen *et al.* 1998, Irmak and Haman 2014).

Note that *PET* is not related to a specific crop. Instead, *PET* corresponds to the ET_0 of a grass lawn during its growing phase that has no water or nutritional restrictions (Verstraeten *et al.* 2008). A crop factor (K_c) should be used to correct *PET* for vegetation other than lawns:

$$PET = K_c\, ET_0 \tag{2.14}$$

Since the evapotranspiration from well-watered agricultural crops may be 10%–30% greater than that from short green grass (Irmak and Haman 2014), it is important to give each vegetation cover unit a realistic but globally estimated crop factor. In hydrology, these corrections are not made at the parcel scale as is usually done in irrigation engineering. There is an extensive body of literature about crop factors in the agronomic and irrigation scientific communities. For example, a K_c larger than 1 is found for full-grown crops with close plant spacing and a large canopy height and roughness. On the other hand, for deciduous fruit trees cultivated without a ground cover crop, K_c values lower than 1 are found resulting from stomata on only the lower side of the leaf and the wide spacing of the trees (for mature trees, only 70% of the ground covered). A set of useful tables and curves can be found in the FAO-56 procedure document (Allen *et al.* 1998). A detailed example of the use of crop factors for wetlands can be found in Stannard *et al.* (2013).

In the same way, stress coefficients (K_s) may account for reductions in *ET* (compared to ET_0 or to $K_c\, ET_0$) resulting from a decrease in the plant transpiration induced by environmental stress (e.g., a lack of available water, air pollution, and soil salinization). Usually, native vegetation does not avoid recurring stressors of different origins. As for crop factors, the ET_0 term of Equation 2.14 may be multiplied with an appropri-ate stress coefficient (Allen *et al.* 1998).

Actual ET estimation

THE THORNTHWAITE WATER BALANCE MODEL

Using *PET* values, a monthly simplified soil water balance model was developed by Thornthwaite and Mather (1955, 1957), and Mather (1969) for deducing the actual *ET* and monthly averaged values for groundwater recharge and runoff. This conceptual simplified model is known as the Thornthwaite water balance model. Assuming that the quantity of water in the soil (and unsaturated zone) can be conceptualized by a single water storage value (S_i) expressed in mm at the end of the month *i* with a given maximum water storage capacity (S_{max}), a monthly accounting procedure is adopted, as described in the flow sheet of Figure 2.6. Moisture is added to or subtracted from S_i depending on whether P_i (precipitation of the month *i*) is greater than or less than PET_i (average potential evapotranspiration of the month *i*). When S_i is increased, its value cannot be greater than S_{max}, and a possible water surplus is generated encompassing the groundwater recharge (R_{gw_i}) and runoff (R_i). On the other hand, when S_i is decreased, its value cannot be lower than zero and a possible water

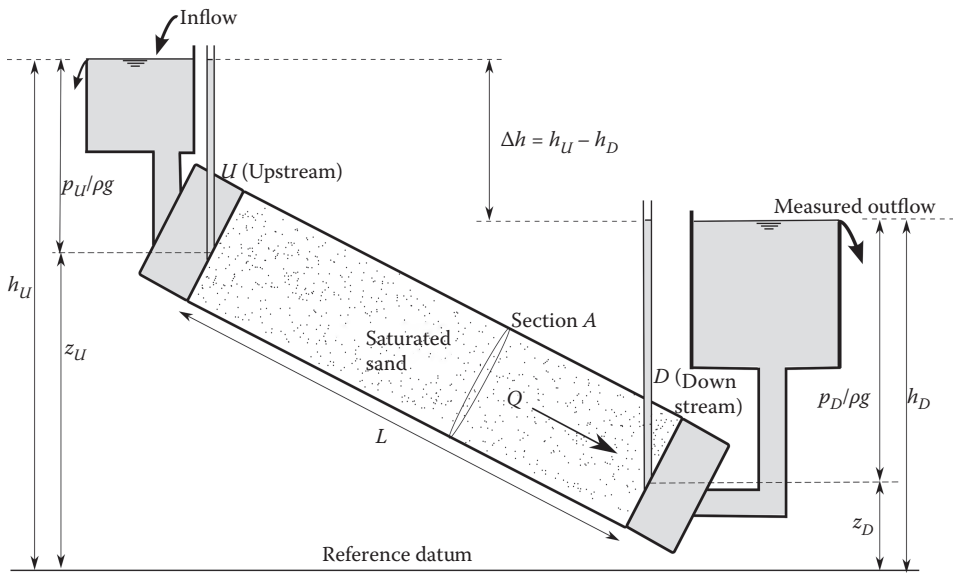

Figure 4.10 Steady groundwater flow as described schematically illustrating Darcy's law. The motion of water is directed from the higher upstream piezometric head toward the lower downstream piezometric head.

In this form, the Darcy's law is similar to Ohm's law of electricity, Fick's law of solute diffusion (see Section 8.2), or to Fourier's law of heat conduction. Indeed, before the advent of numerical models, many groundwater flow problems were solved using physical models involving electricity or heat conduction analogies.

Groundwater flow takes place from a higher piezometric head to a lower one ($\Delta h = h_U - h_D$) (Figure 4.10), with h_U and h_D respectively the upgradient and downgradient piezometric heads, as groundwater flow requires energy (Delleur 1999). It should be noticed that groundwater flow is not necessarily directed from a higher to a lower *pressure*. As shown in Figure 4.10, flow can be in the direction of increasing pressure ($p_D > p_U$) but is always in the direction of decreasing piezometric head. This phenomenological law, expressed in terms of piezometric heads, is valid for an incompressible fluid (i.e., with a constant density). If the study case involves varying density of water due to solute concentrations or (geo) thermal effects, the state variable should be the pressure (as mentioned previously in Section 4.3).

Specific discharge and velocities

One of the primary uses of Darcy's law is to calculate a *specific discharge*, dividing the flow rate by the cross-sectional area of the porous medium:

$$q = \frac{Q}{A} = K\frac{\Delta h}{L} \tag{4.20}$$

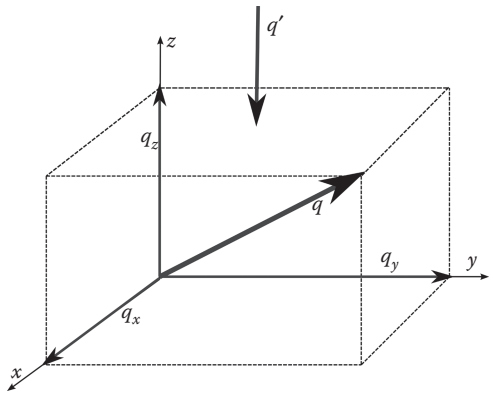

Figure 4.24 Groundwater mass conservation for a volume of saturated geological medium under steady-state conditions.

unit volume of porous medium and per unit time. For saturated groundwater flow, it is written:

$$-div(\rho \boldsymbol{q}) = -\nabla \cdot (\rho \boldsymbol{q}) = -\rho q' \tag{4.47}$$

where $div(\boldsymbol{q}) = \nabla \cdot \boldsymbol{q} = ((\partial q_x/\partial x) + (\partial q_y/\partial y) + (\partial q_z/\partial z))$ in the 3D saturated medium (Figure 4.24), q' (s^{-1}) [T^{-1}] is the water flow rate per unit volume of the geological medium that is injected ($q' > 0$) or withdrawn ($q' < 0$). The term q' is often called the "source" or "sink" term, also referred to as the "stress" ("perturbation") term of the groundwater flow equation.

Entering the Darcy law Equation 4.28 in the Equation 4.47 leads to the following 3D equation:

$$\nabla \cdot (\rho \boldsymbol{K} \cdot \nabla h) + \rho q' = 0 \tag{4.48}$$

and

$$\nabla \cdot \left(\rho \frac{\boldsymbol{k}}{\mu} \cdot (\nabla p + \rho g \nabla z) \right) + \rho q' = 0 \tag{4.49}$$

The different terms of these equations are in units of kg/(m^3s) [$ML^{-3}T^{-1}$] expressing the mass of flowing water per volume of porous medium per second. Equation 4.47 written in indicial notation is:

$$\frac{\partial}{\partial x_i} \left(\rho K_{ij} \frac{\partial h}{\partial x_j} \right) + \rho q_i' = 0 \tag{4.50}$$

Note that this equation can be written under different simplified forms. The most classical is the following:

$$\frac{\partial}{\partial x} \left(K_{xx} \frac{\partial h}{\partial x} \right) + \frac{\partial}{\partial y} \left(K_{yy} \frac{\partial h}{\partial y} \right) + \frac{\partial}{\partial z} \left(K_{zz} \frac{\partial h}{\partial z} \right) + q' = 0 \tag{4.51}$$

then the first term on the right-hand side of Equation 4.61 is written:

$$n\frac{\partial \rho}{\partial t} = n\frac{\partial \rho}{\partial p}\frac{\partial p}{\partial t} = n\rho\beta_w \frac{\partial p}{\partial t} \tag{4.64}$$

If we assume that the total stress remains unchanged (i.e. $\partial\sigma = 0$; see Chapter 6) then taking the derivative of Equation 4.57 gives:

$$\frac{\partial \sigma'}{\partial t} = -\frac{\partial p}{\partial t} \tag{4.65}$$

One must recall that

$$n = \frac{V_p}{V} \quad \text{and} \quad (1-n) = \frac{V_s}{V} \tag{4.66}$$

where V_p and V_s are respectively the pore and solid volumes in the REV.

The second term on the right-hand side of Equation 4.61 can be expanded as:

$$\rho\frac{\partial n}{\partial t} = \rho\frac{(V_p + V_s)(\partial V_p/\partial t) - V_p((V_p + V_s)/\partial t)}{V^2} \tag{4.67}$$

and simplified using Equations 4.66 and if the solid compressibility is neglected ($\partial V_s/\partial t \cong 0$), then:

$$\rho\frac{\partial n}{\partial t} = \rho\frac{V_s(\partial V/\partial t)}{V^2} = \rho\frac{(1-n)}{V}\frac{\partial V}{\partial t} = \rho\frac{(1-n)}{V}\frac{\partial V}{\partial \sigma'}\frac{\partial \sigma'}{\partial t} \tag{4.68}$$

Using Equation 4.65, and the definition of the volume compressibility (Equation 4.58), gives:

$$\rho\frac{\partial n}{\partial t} = \rho(1-n)\alpha\frac{\partial p}{\partial t} \tag{4.69}$$

With Equations 4.64 and 4.69, Equation 4.61 becomes:

$$\frac{\partial(\rho n)}{\partial t} = \rho\{n\beta_w + (1-n)\alpha\}\frac{\partial p}{\partial t} \tag{4.70}$$

The first term vanishes if the water compressibility is also assumed negligible ($\beta_w \cong 0$) with regards to the volume compressibility.

Now, entering this water storage variation in the mass balance equation, and expressing that the Darcy specific discharge is here in fact a relative discharge with respect to a moving solid, Equation 4.55 can be rewritten as:

$$\nabla \cdot \rho(\boldsymbol{q}_r + n\boldsymbol{v}_s) - \rho q' = -\rho\{n\beta_w + (1-n)\alpha\}\frac{\partial p}{\partial t} \tag{4.71}$$

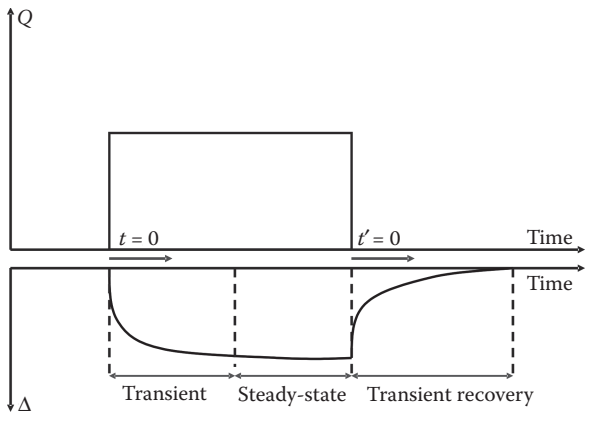

Figure 5.4 Measured drawdown (Δ) function of time for a constant pumping rate. Transient data are measured before a stabilization of piezometric heads corresponding to steady-state data (if the pumping rate is not too high). During the recovery phase, the rising back up of the heads toward the initial static piezometric level also corresponds to transient data.

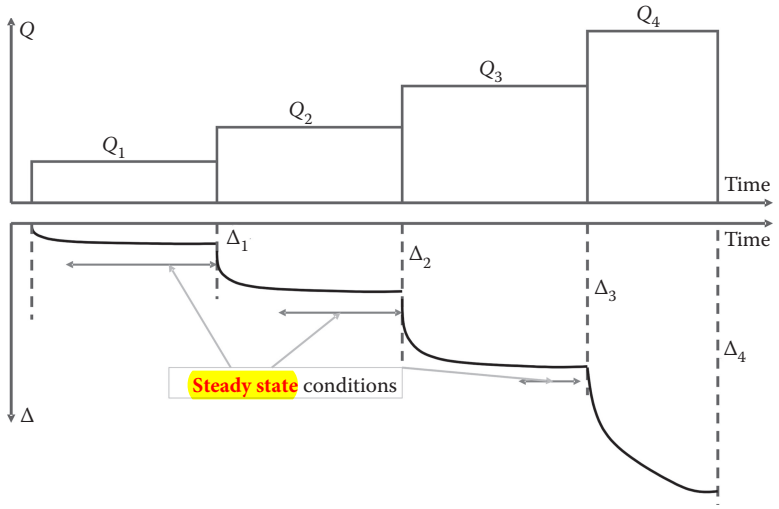

Figure 5.5 Measured drawdown function of time for a step-drawdown pumping test. For each pumping step, the measured drawdown takes more and more time to reach a stabilized value.

the specific storage coefficient or storage coefficient, and a few important additional data as the influence radius and the critical discharge rate of the pumping well. Note that interpretation of pumping tests yields parameters averaged over a domain of uncertain extent (Pechstein *et al.* 2016) with the important assumption of homogeneity of this influenced domain. Consequently, equivalent hydraulic conductivity values from a pumping test can be time dependent as function of the heterogeneity scale.

At any point at a distance r from the pumping well:

$$(h_0^2 - h^2) = \frac{Q}{\pi K} \ln \frac{R}{r} \tag{5.26}$$

Using the measured drawdown in the unconfined aquifer, $\Delta = (h_0 - h)$ and consequently $(h_0^2 - h^2) = 2h_0\Delta - \Delta^2$, Equation 5.26 written as function of the constant discharge rate becomes:

$$Q = \frac{\pi K(2h_0\Delta - \Delta^2)}{\ln(R/r)} \tag{5.27}$$

One can observe that if $\Delta' = \Delta - \Delta^2/2h_0$, we can choose to express this Equation 5.27 as follows:

$$Q = \frac{2\pi K h_0(\Delta')}{\ln(R/r)} \tag{5.28}$$

That is similar to Equation 5.21, with a transmissivity calculated over the initial saturated thickness $T = Kh_0$. So, in unconfined aquifers and provided that the drawdown is limited (see above), one can use equations established for confined conditions replacing Δ by Δ' (Kruseman and de Ridder 1994).

If the piezometric head is measured in the pumping well (at a distance r_w) and at some point close to the well (at a distance r), Equation 5.26 is written as:

$$(h^2 - h_w^2) = \frac{Q}{\pi K} \ln \frac{r}{r_w} \tag{5.29}$$

And between two points located at distances r_1 and r_2 from the pumping well:

$$(h_2^2 - h_1^2) = \frac{Q}{\pi K} \ln \frac{r_2}{r_1} \tag{5.30}$$

As a function of the constant discharge rate, the Dupuit's equation is most often written as:

$$Q = \frac{\pi K(h_2^2 - h_1^2)}{\ln(r_2/r_1)} \tag{5.31}$$

In practice, a direct application is made of Equation 5.26 in:

$$(h_0^2 - h^2) = \frac{0.73\,Q}{K} \log R - \frac{0.73\,Q}{K} \log r \tag{5.32}$$

Therefore in a $(\log r, (h_0^2 - h^2))$ diagram, the slope of the best fitted line (Figure 5.9) will provide $(0.73\ Q/K)$ and thus K can be deduced. The fitted line can be prolonged

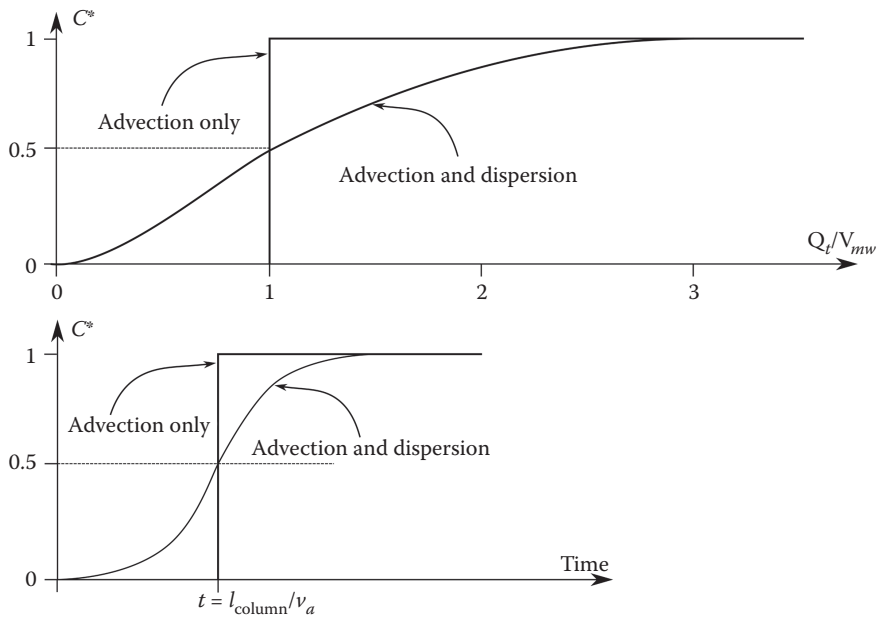

Figure 8.5 Solute breakthrough curve as obtained in a 1D column of homogeneous porous medium for a continuous injection of solute under steady-state saturated groundwater flow. Relative concentrations are used where $C^* = (C - C_0)/(C_{max} - C_0)$ with $0 < C^* < 1$. For such standardized column tests, it is usual to express time in dimensionless units, multiplying the time (t) by the ratio between the total discharge (Q) and the mobile water pore volume of the column ($V_{mw} = n_m V_t$): Qt/V_{mw} (also referred to as "pore volumes" or PV's). (Modified from Bear, J. and A.H.D. Cheng. 2010. *Modeling groundwater flow and contaminant transport*. Springer; Pinder G.F. and M.A. Celia. 2006. *Subsurface hydrology*. Hoboken, New Jersey: Wiley & Sons.)

dependent on the velocity components and dispersivities characterizing the geological medium at the considered scale. In 3D, the 9 components of this tensor can be calculated as a function of the velocity components and the two main *dispersivities* which are: a_L and a_T respectively the *longitudinal* and *transverse dispersivities* expressed in m [L] (Scheidegger 1961, Bear 1972):

$$D_{ij} = (a_L\text{-}a_T)\frac{v_{a_i} v_{a_j}}{|v_a|} + a_T |v_a| \delta_{ij} \tag{8.13}$$

where indicial notations are used and i and $j = 1, 2$ or 3 respectively, δ_{ij} is the Kronecker function with $\delta_{ij} = 1$ if $i = j$ and $\delta_{ij} = 0$ if $i \neq j$, $|v_a| = \sqrt{(v_{a_1}^2 + v_{a_2}^2 + v_{a_3}^2)}$. Burnett and Frind (1987) (cited by Schwartz and Zhang 2003, Bear and Cheng 2010, among many others) also developed this equation but as a function of three main dispersivities, differentiating between a_{TH}, and a_{TV}, respectively the transverse horizontal and transverse vertical dispersivities. Also, Lichtner *et al.* (2002) introduced a 4-component form, where the longitudinal and transverse dispersivities vary depending on the flow

A dimensionless *Peclet number* is used to provide a ratio between the rates of solute transport by advection and dispersion (Bear and Cheng 2010). This *Peclet number* (Box 8.2) is often used to characterize the relative importance of these two transport processes. When advection dominates, mechanical dispersion is far more important than diffusion thus diffusion can be neglected. When advection is weak, diffusion can become more important than mechanical dispersion.

Box 8.2 Peclet number for solute transport

A dimensionless Peclet number was initially defined by:

$$Pe = \frac{v_a l}{D_m} = \frac{q l}{n_m D_m}$$

where $v_a = q/n_m$ is the velocity, D_m is the effective diffusion coefficient and l is a "characteristic" length of the problem (Freeze and Cherry 1979). Unfortunately, different Peclet number definitions exist and, for a given particular case, they lead to diverse values (Huysmans and Dassargues 2005). In particular, there are significant differences in the definition of the "characteristic" length such as the characteristic length of the pores (Bear and Verruijt 1987), hydraulic radius of the saturated pore space (Bear and Cheng 2010), $\sqrt{k}$ with k the intrinsic permeability (de Marsily 1986), average grain size, the correlation scale assuming a Gaussian correlation structure of the medium heterogeneity, or the distance from the injection source (lab and field tracer tests). Note that not all of the possible differences in the l definitions are due to the scale of study. In very low permeability environments (e.g., as in plastic clays or claystones in the context of radioactive waste storage), it could be very useful to assess if transport by advection and dispersion are to be neglected compared to diffusion. It is often considered that if $Pe \ll 1$, dif-fusion dominates. To this end, and with this objective in mind, different definitions of the Pe number were tested by Huysmans and Dassargues (2005). Generalizing this approach, for analytical interpretation of tracer tests, Sauty (1980) defined a *Peclet number* as the ratio between advection and dispersion as follows:

$$Pe = \frac{v_a L}{D}$$

where L is the distance from the point of injection to the point of measurement of the tracer test, and D is the hydrodynamic dispersion (including diffusion).

An important point to observe is that dispersion is an anisotropic process. If a porous medium is anisotropic, the anisotropy of the medium is added to the anisotropy of the mechanical dispersion and the dispersion tensor $\boldsymbol{D}$ becomes a fourth-order tensor with 81 components:

$$D_{ij} = \sum_{k=1}^{3}\sum_{m=1}^{3} a_{ijkm} \frac{v_{a_k} v_{a_m}}{|v_a|} \tag{8.15}$$

Table 8.1 Individual equilibrium dissolved concentrations (C_i^v in mg/L) and pure solubility for different BTEX compounds of a given gasoline mixture (with a global averaged molecular weight of 101 g/mole)

Compound	*Chemical formula*	*% in weight in mixture*	X_i	C_i^v	S_i^o	*Molecular weight*
Benzene	C_6H_6	3	0.039	69.04	1780	78.12
Toluene	C_7H_8	20	0.219	113.99	520	92.15
Ethylbenzene	C_8H_{10}	2.5	0.024	4.28	180	106.18
m-, p-xylenes	C_8H_{10}	12	0.114	18.26–21.69	160–190	106.18
o-xylenes	C_8H_{10}	3	0.029	4.99	175	106.18
MTBE	$(CH_3)_3COCH_3$	9	0.103	4639	45,000	88.17

Sources: Modified from Fitts, Ch. R. 2002. *Groundwater science*. Academic Press; Citing Cline, P.V., Delfino, J.J. and P.S.C. Rao. 1991. *Environmental Science and Technology* 25(5): 914–920.

NAPL affinity for solids and groundwater

The mobility of an organic contaminant under the form of an NAPL in groundwater is influenced by its "affinity" for soil particles or matrix solids. The ratio between the NAPL solubility in octanol and its solubility in water is used to provide a relative affinity:

$$K_{ow} = \frac{S^o_{NAPL\ in\ octanol}}{S^o_{NAPL\ in\ gw}} \tag{8.66}$$

where K_{ow} is the octanol-water partition coefficient (-) measuring hydrophobicity. Organic contaminants characterized by a high K_{ow} are generally retained on the solid matrix and thus quasi-immobile in the porous medium except if the NAPL pressure in the pores is sufficiently high, for example, in the case of a thick layer of NAPL.

If the natural organic content of the geological medium is not negligible, the nonpolar organic contaminant can sorb onto the natural organic fraction of the solid matrix (for more details about sorption see Section 8.2). An organic carbon-water partition coefficient can be defined as:

$$K_d = f_{oc} K_{oc} = f_{oc} \left(\frac{\bar{C}_{NAPL}}{S^o_{NAPL\ in\ gw}} \right) \tag{8.67}$$

where f_{oc} is the organic matter fraction (i.e., the quantity of natural organic matter in the REV matrix) [ML^{-3}], K_{oc} is the ratio of the adsorbed NAPL onto the matrix ($\bar{C}_{NAPL}$) on the dissolved NAPL in groundwater (taken equal to its solubility in groundwater ($S^o_{NAPL\ in\ gw}$) in the REV [ML^{-3}]).

Vapor mobility of NAPL organic contaminants

In the partially saturated zone, the NAPL vapor pressure ($p_{NAPL\ vapor}$) determines the equilibrium pressure of the gas phase in contact with the liquid NAPL phase. If an NAPL has a high vapor pressure, it is highly volatile and belonging to the VOCs (volatile organic compounds) family of contaminants.

Depending on the objectives, injection can be performed (a) at the top of the well with a volume of additional water, (b) by a small diameter tube through a packer, (c) by perforated small diameter tubes, or (d) with a uniform spatial distribution of the tracer concentration by recirculation (Maliva, 2016).

Sampling procedures and techniques have also evolved significantly over the past few years. Indeed, when a BTC is analyzed, one must know how the sample was obtained. Is the sample from a pumping well with full screens inducing "depth-averaged" conditions? Or is it a BTC from a point sampling device between packers (or between bentonite packs) or from another type of multilevel sampling device? Depending on the tracer test configuration and objectives, passive samplers can be placed in combination with sequential automatic samplers and/or down-hole devices as, for example, fluorometers. Indeed, passive samplers provide only a cumulative value of adsorbed tracer mass, while automatic samplers followed by lab analysis provide very accurate tracer concentrations at given times, and down-hole fluorometers allow more frequent or nearly continuous measurements of a given fluorescent tracer. Combined with the sampling procedure, hydrogeophysical measurements can also be performed especially with tracers having an influence on the electrical resistivity (Hermans *et al.* 2012). Time-lapse hydrogeophysics applied to tracer experiments (Hermans *et al.* 2015) and to the characterization of preferential pathways at contaminated sites is a rapidly developing topic. As mentioned previously (see Dispersion paragraph in Section 8.2), these high-resolution measurement techniques are very useful to constrain inverse modeling procedures.

8.6 Transport and residence times

It has always been a dream for hydrogeologists to be in a position to determine exactly the "age" of a drop of water. Indeed, many important groundwater management decisions could be based on knowing locations of "young" and/or "old" groundwater. For example, old groundwater in an aquifer could indicate a relatively low current recharge rate (e.g., with regards to pumped groundwater). In contamination problems, the time required for a plume to reach a pumping well or any "target" zone to be protected is crucial. The relative importance of reactive transport, adsorption, and degradation processes influencing solute transport could be highly dependent on the time spent by contaminated water in the partially saturated and saturated zones in contact with the mineral heterogeneity of the geological medium. Determining legacy contamination sources (e.g., agricultural practices, industrial activities) which have led to contamination, is another application where groundwater age can be very useful.

If we follow a drop of water, age is an evolving variable with time, meaning the difference between an initial moment and the determination moment. With this concept, age is linked to an individual entity not mixing with anything else during the whole journey. In short, this important assumption means that age of groundwater is an idealized concept, or at least a misleading term, as it neglects mixing.

Piston-flow groundwater age: an idealized concept

Conceptually, if we imagine an infinitely small water parcel, unaffected by mixing processes, the idealized age between an initial moment and the present moment can

On the basis of many measurements from the "Global Network of Isotopes in Precipitation" (GNIP) established by IAEA and WMO, Craig (1961) observed that there is a strong and general correlation between ^{18}O and D in global freshwaters (i.e., on the average global scale). The regression line of this correlation (with r^2 better than 0.95) gives the "*global meteoric water line*" (GMWL), defined by (Figure 8.28):

$$\delta D = 8\delta^{18}O + 10‰ \tag{8.76}$$

This is a global regression line which represents the alignments of changes in isotopic compositions of ^{18}O and D with precipitation. Similarly, due to the combined effects described above, the relationship between $\delta^{18}O$ and δD in rainfall can be plotted for a specific area on a local meteoric line (LMWL). The relationship can also be specific for some periods (such as seasons). As mentioned before, this LMWL is needed for any further interpretation of groundwater isotope ratios in terms of mixing and origins.

Groundwater analysis results not lying on this line imply the groundwater has undergone processes (i.e., often named "secondary processes" in the isotope community) which have modified this correlation. In a ($\delta^{18}O$, δD) diagram, the effect of each process is reflected by a line segment joining the point of the initial composition and the point representing the composition of the water having undergone the considered process (Figure 8.28). Without entering into too much detail about isotope fractionation, one can summarize the following influences on the $\delta^{18}O$ and δD ratios (Figure 8.28):

- Evaporation makes the remaining surface water or groundwater enriched in both heavy isotopes. In the ($\delta^{18}O$, δD) diagram, the evaporating groundwater line is below the local MWL having a slope of 2–3 while the evaporating surface water line has a slope of 4–6.

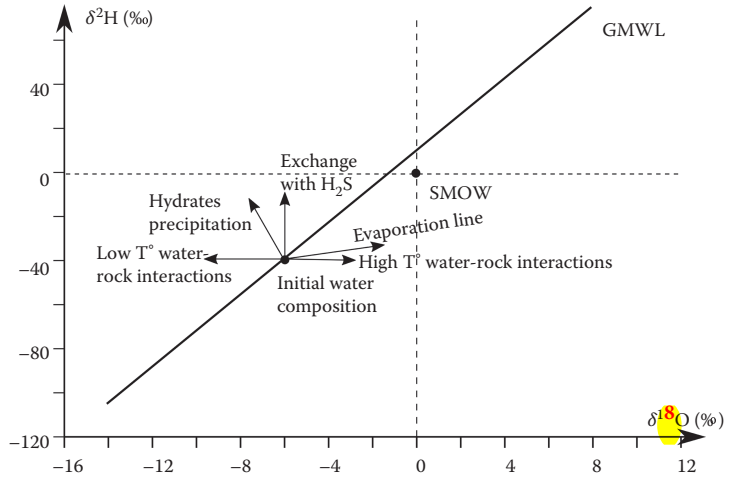

Figure 8.28 Relation between the $\delta^{18}O$ and δD values, showing the GMWL and deviation from this line for different processes that water undergoes. (Modified from Gascoyne, M. and T. Kotzer. 1995. *Isotopic methods in hydrogeology and their application to the underground research laboratory.* Manitoba. Chalk River Laboratories, A.E.C.L. - 11370, Chalk River.)

- During water-rock interaction, especially with calcite and silicates. δD is not affected since H is rarely present in the minerals composition. However, δ^{18}O is modified and is highly dependent on temperature so that this "isotopic thermometer" is used for geothermal groundwater studies. At high temperature the positive δ^{18}O can be significant, while at low temperatures (<100 °C) water-rock interactions induce only a slight decrease of δ^{18}O.
- Precipitation of hydrated minerals increases δD and decreases δ^{18}O since many of these minerals (clay, gypsum) are enriched in ^{18}O and depleted in ^{2}H.
- Isotopic exchange with NAPLs and gas species such as H_2S does not change δ^{18}O but increases the presence of ^{2}H in groundwater, thus increases δD.

An illustration of some of these effects is given in Figure 8.29 with, on one hand, groundwaters showing typical (δ^{18}O, δD) signatures of evaporated remaining waters and, on the other hand, groundwaters showing depleted δ^{18}O due to a low temperature exchange with CO_2 from a magmatic origin.

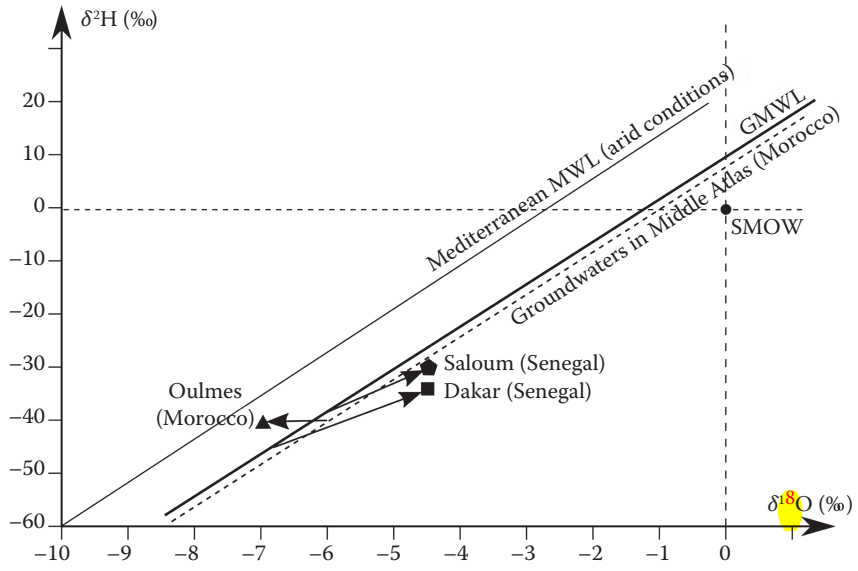

Figure 8.29 Relation between (δ^{18}O, δD) values for the evaporation influenced Saloum groundwaters (from Ndeye, M.D., Orban, P., Otten, J., Stumpp, C., Faye, S. and A. Dassargues. 2017. *Journal of Hydrology Regional Studies* 9: 163–182) and Quaternary groundwaters near Dakar (from Madioune, D.H., Faye, S., Orban, P., Brouyère, S., Dassargues, A., Mudry, J., Stumpp, C. and P. Maloszewski. 2014. *Journal of Hydrology* 511: 443–459), contrasting with the Oulmes groundwaters influenced by low temperature exchanges with CO_2 of magmatic origin (from Wildemeersch, S., Orban, P., Ruthy, I., Grière, O., Olive, P., El Youbi, A. and A. Dassargues. 2010. *Environmental Earth Science* 60(8): 1753–1769). For these three regions, precipitation compositions correspond or are very close to the GMWL showing an Atlantic Ocean origin. Note that a regional Middle Atlas (Morocco) groundwater line is found slightly below the GMWL.

and τ is the time (in days) or ^{222}Rn-based residence time $\tau_{^{222}\mathrm{Rn}}$ (i.e., apparent age). This last term can thus be obtained by:

$$\tau_{^{222}\mathrm{Rn}} = \left(\lambda_{^{222}\mathrm{Rn}}\right)^{-1} \ln\left(1 - \frac{A_{^{222}\mathrm{Rn}\,meas}}{A_{^{222}\mathrm{Rn}\,eq}}\right) \tag{8.81}$$

Interpretation becomes problematic for ^{222}Rn residence times longer than 12 days ($\sim$3 half-lives) as measured and equilibrium ^{222}Rn activity concentrations converge toward very similar values (e.g., Cecil and Green 2000, Schilling 2017, Schilling *et al.* 2017).

Schilling *et al.* (2017) proposed to complement ^{222}Rn measurements by ^{37}Ar to close the residence time gap characterization between a few days and a few tens of days (Figure 8.32).

Argon -37 with a half-life of 35.1 days is a very rare radioactive tracer that is now measurable at natural levels (Loosli and Purtschert 2005). Recent progress in low level detection and water sample reduction has increased field application for groundwater dating. Without entering in details, the production of ^{37}Ar in the subsurface (mainly due to Ca activation by cosmic rays) can be considered as reaching a peak between 2 and 4 m depth and then decreases with depth (more details can be found in Riedmann and Purtschert 2011). Thus, the ^{37}Ar production-decay equilibrium activity concentration depth profile must be known to use this technique for further assessment of groundwater residence times (especially for recently infiltrated waters). Similar to ^{222}Rn, but including activity concentration dependency with depth (i.e., decreases with depth), ^{37}Ar-based residence time $\tau_{^{37}\mathrm{Ar}}$ (i.e., apparent age) can be obtained (Cecil and Green 2000) by:

$$A_{^{37}\mathrm{Ar}\,meas}(d) = A_{^{37}\mathrm{Ar}\,eq}(d)\left(1 - e^{-\lambda_{^{37}\mathrm{Ar}}\tau}\right) \tag{8.82}$$

where $A_{^{37}\mathrm{Ar}\,meas}(d)$ and $A_{^{37}\mathrm{Ar}\,eq}(d)$ are respectively the measured and equilibrium activity concentrations of ^{37}Ar at the depth d, $\lambda_{^{37}\mathrm{Ar}}$ is the degradation constant equal to 0.0197 (in days^{-1}), and τ is the time (in days) or ^{37}Ar-based residence time $\tau_{^{37}\mathrm{Ar}}$ (i.e., apparent age). This last term can thus be obtained by:

$$\tau_{^{37}\mathrm{Ar}} = \left(\lambda_{^{37}\mathrm{Ar}}\right)^{-1} \ln\left(1 - \frac{A_{^{37}\mathrm{Ar}\,meas}(d)}{A_{^{37}\mathrm{Ar}\,eq}(d)}\right) \tag{8.83}$$

The reasoning is similar to that as previously given, considering a zero starting point at the surface (atmospheric conditions) and an increase in ^{37}Ar concentration over 100 days ($\sim$3 half-lives) in the first few meters. A negative exponential evolution of the activity concentration is added to account for the ^{37}Ar decrease as a function of depth (Schilling 2017, Schilling *et al.* 2017).

8.8 Vulnerability and protection of groundwater

Facing groundwater contamination threats from anthropogenic and natural origins, prevention is always more effective then remediation. Sustainable management of

Using the Bernoulli equation (Equation 4.16), this can also be written as a function of the pressure head. The *capillary head* or *suction head* (h_c) is defined as:

$$\psi = h_c = \frac{p_c}{\rho g} = -h_p = -\frac{p}{\rho g} = z - h \tag{9.4}$$

where h_p is the pressure head.

Capillary pressure is considered to be a nonnegative value, but when the continuity between the saturated and partially saturated medium is considered in further equations, the main variable will be the water pressure (or the pressure head) that therefore takes negative values in the vadose zone. In other words, as the water content decreases, the capillary pressure increases, and the pressure head becomes more negative (Schwartz and Zhang 2003). This negative water pressure could be interpreted as the pressure that would be needed to extract water from the partially saturated medium. This negative pressure is typically measured using *tensiometers* generally consisting of a water-filled tube with a porous ceramic cup at one end. A partial vacuum can be created in the tube by a hand pump to subtract the air. The water in the tube is pulled out by the pressure conditions in the partially saturated medium, increasing the vacuum inside the tube measured by the pressure sensor. After a while, the water pressure in the tensiometer is considered to be in equilibrium with the soil water pressure.

For a given geological medium (i.e., lithology), it is important to obtain information about the *water retention curves* (i.e., equivalent to *capillary pressure (or head)—water (or moisture) content* curves) (Figure 9.2) or, alternatively, the *capillary pressure (or head)—saturation* curves.

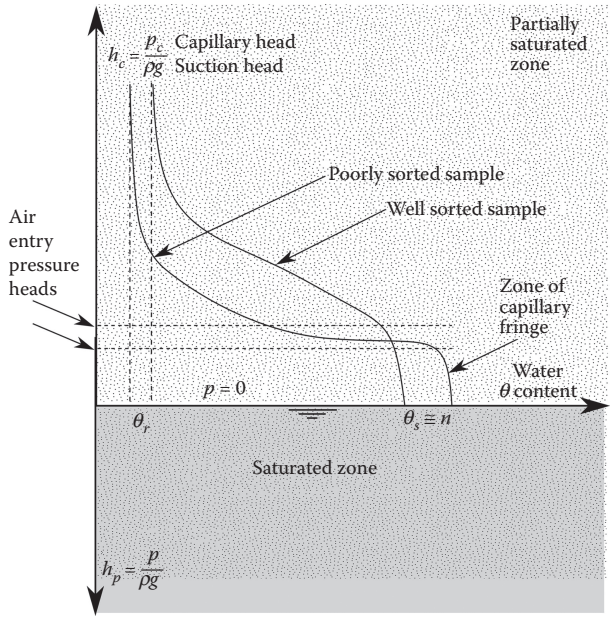

Figure 9.2 Typical schematic retention curves (i.e., capillary pressure head curve) for poorly and well-sorted porous media.

Typical curves are shown in Figure 9.2 for well sorted and poorly sorted porous media. For saturated conditions, the maximum water content is reached and considered equal to the total porosity $\theta = \theta_s = n$ and $S = S_{max} = 1$, neglecting the entrapped air. As the suction first increases, the water content remains near the full saturation. To obtain a significant desaturation, an increase in the suction above a threshold value is necessary. This pressure threshold is named *air-entry pressure* head or bubbling pressure, and it depends on the pore size. In a vertical profile of the porous medium, these conditions occur in the *capillary fringe* (see Chapter 1). Then, effective desaturation corresponds to the drain-age of the medium under increasing suction conditions (i.e., decreasing water pressure), and this drainage is more rapid for large pores than small pores. For greater suction values, the curve derivative tends to the infinite (i.e., vertical asymptotic line). Therefore, an additional increase of the suction does not significantly change the *residual water content* (θ_r), corresponding to the *residual saturation* (S_r).

For practical purposes, the water content and the water saturation are often normalized with respect to the variation range in the medium:

$$\Theta = \frac{\theta - \theta_r}{\theta_s - \theta_r} \tag{9.5}$$

$$S_e = \frac{S - S_r}{1 - S_r} \tag{9.6}$$

where Θ is defined as the (normalized) effective water content, and S_e is defined as the (normalized) effective saturation. Retention curves obtained for each characterized porous medium express $\Theta(h_p)$ or $S_e(h_p)$.

Theoretically, these curves are used to determine, at any given time, the amount of water retained in the partially saturated medium for a given pressure or head. However, in practice, they are strongly affected by hysteresis and thus the direction and history of drainage and wetting. These processes are induced by (Bear and Verruijt 1987): "ink-bottle" effects resulting from the various shapes of the pores; "raindrop" effects resulting from a larger contact angle for the advancing (compared to the receding) water-air interface on a solid surface; air entrapment, particularly during rewetting; and various geomechanical effects (i.e., consolidation, swelling, and shrinkage). Many studies have been reported about hysteresis processes in air-water, oil-water, and gas-oil systems in each of the specialized bodies of literature. However, for evident simplifying reasons, only an average curve (sometimes only the drainage curve) is most often considered in practice (Bear and Cheng 2010).

Another problem comes from the heterogeneity of the partially saturated zone and the *saturation jumps* that this heterogeneity can induce in the corresponding vertical profile (Figure 9.3). These create many difficulties (see Section 9.3) because jumps in the hydraulic parameters values are consequently induced.

9.3 Partially saturated flow

Hydraulic conductivity under partially saturated conditions

For a given REV of a partially saturated porous medium, hydraulic conductivity varies with the water content and thus as a function of the water pressure head.

water consumption of deep roots actually stabilizes the depth of the piezometric levels. In cleared zones, piezometric variations can be more important than in uncleared zones, demonstrating greater responses to rainfall events and inducing more evaporation periods (Peck and Williamson 1987). Combined with irrigation, the excess water contributes to the rising of the water table and, consequently, to more salinization (as explained above).

Box 10.1 Increasing salinity in groundwater and streams resulting from irrigation in the arid zone of the southern flank of the Atlas Mountain range in Morocco

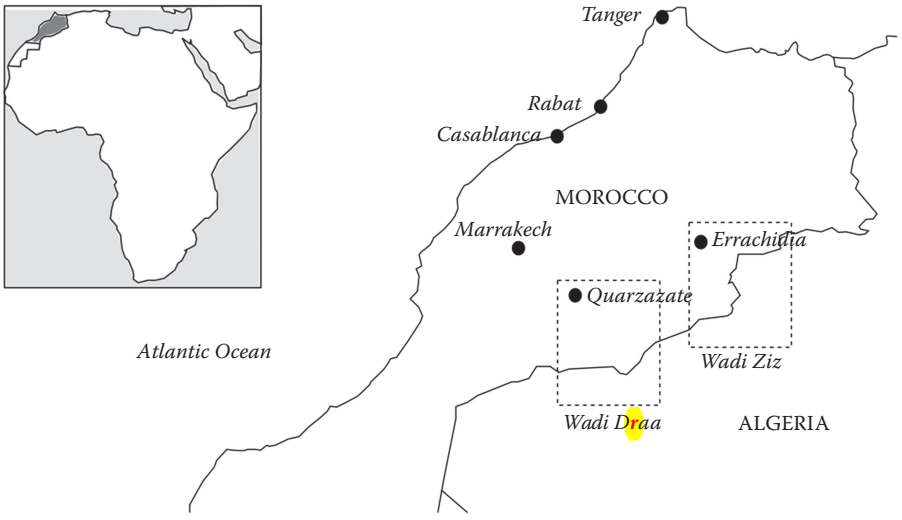

The valleys of the Drâa and Ziz wadis on the southern flank of the central Anti-Atlas Mountains (Morocco) represent a particularly serious salinization problem resulting from irrigation. The Drâa and Ziz wadis flow southward reaching their southernmost points adjacent to the Sahara foreland (Klose 2012). Irrigation is needed for basic cereal crops, and in particular, the date palm trees grown in a series of oases located along the main wadis. Both the surface water of the wadis (i.e., released from dams located upstream) and the groundwater are used for irrigation. Water from the southern flank of the high Atlas Mountain range is collected by the El Mansour Eddahbi dam in Ouarzazate (the upper Drâa) and the Hassan Addakhil dam near Errachidia (the upper Ziz) (see map). Water from these dams has a nonnegligible salt content from evaporite dissolution in the southern foothills of the Atlas range, as well as from evaporation in the dam reservoirs. Irrigation occurs using water released from the dams in the wadis and is organized in the oases through complex networks of traditional canals named "seguias." If the released water is not sufficient or occurs at an inappropriate time for the crops, local groundwater pumping takes place in the alluvial aquifers corresponding to the different palm oases using thousands of shallow wells. The chain of processes described in Figure 10.1 is triggered, resulting in a

NEUMANN BOUNDARY CONDITIONS

A Neumann-type BC or second-type transport BC corresponds to prescribing the value of the normal derivative of the concentration on a given boundary:

$$\nabla C^v \cdot \boldsymbol{n} = \frac{\partial C^v}{\partial n}(x,y,z,t) = g''(x,y,z,t) \tag{12.10}$$

where $g''(x, y, z, t)$ is a known function dependent on coordinates x, y, z and possibly also on time. In fact, associated to local values of the effective diffusion coefficient and dispersivities, it corresponds to a prescribed hydrodynamic dispersion mass flux across the boundary (see Equation 8.16):

$$\boldsymbol{n} \cdot (-n_m \boldsymbol{D_h} \cdot \nabla C^v) = -n_m D_{h,n} \frac{\partial C^v}{\partial n}(x,y,z,t) = q''(x,y,z,t) \tag{12.11}$$

where $q''(x, y, z, t)$ is the prescribed hydrodynamic dispersion mass flux normal to the boundary (this can be different from one time step to another), $D_{h,n}$ is the dispersion in the direction normal to the boundary.

It is usually hard to assess a nonzero hydrodynamic dispersion mass flux to be prescribed on a boundary. So, this type of BC is essentially used for prescribing a zero-dispersion flux through a boundary by using $\partial C^v/\partial n = 0$. Associated to a zero Neumann BC for flow, it then corresponds to a totally impervious boundary. On the other hand, when combined with a prescribed head (Dirichlet BC for flow), only an advective mass flux is allowed across the boundary. In the case shown in Figure 12.13, both upgradient and downgradient BCs for flow are prescribed heads with the other

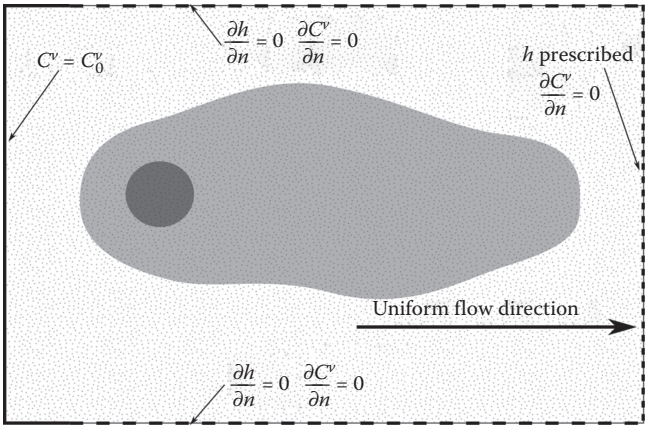

Figure 12.13 On the same example than in Figure 12.12, Neumann transport BCs prescribing a zero-hydrodynamic dispersion mass flux through the boundary ($\partial C^v/\partial n = 0$). Combined with a prescribed head (Dirichlet BC for flow), only an advective mass flux is allowed across the downgradient boundary (on the right-hand side of the figure). Combined with zero Neumann BCs for flow ($\partial h/\partial n = 0$), totally impervious BCs are prescribed.

subsurface data domain (Huysmans and Dassargues 2009). Construction of suitable training images is critical. They should be representative of the geological heterogeneity and large enough to be statistically characterized. Training images are bound by the principles of stationarity and ergodicity (Caers and Zhang 2004). More and more complex data can be integrated in the choice of the training images through the use of learning processes. High computing costs are linked to pixel-based training image and MPS algorithms (Pirot 2017). Cloud computing, analogs, and the use of "clever tools" to include data more efficiently are needed (Rezaee *et al.* 2015, Pirot *et al.* 2017) and this research area is in full development.

12.7 Prediction focused approaches based on Bayesian evidential learning

As mentioned previously (see Section 12.5), if a detailed sensitivity approach includes directly the forecast (White 2017), not only historical data are used (as for model calibration), but also the uncertainty of predictions, for influencing the conceptual and main parameters to be considered for inversion. Here, the general workflow of groundwater modeling is changed introducing directly the simulation of prediction scenarios for detecting what are the parameters producing the largest uncertainty in the results. These parameters are then the priority of the inverse procedure. This is an efficient way of keeping only the forecast-sensitive input datasets for multiple conceptual model and parameters analysis (Kikuchi *et al.* 2015).

Recently, new ideas appeared giving less importance to the calibration or inverse modeling procedure. Revisiting the relations between data, models, results, and decision-making (Ferré 2017), the predictive ability of a groundwater model is defined as the first and unique priority in prediction-focused approaches (PFA) developed by Hermans *et al.* (2016). Inversion is replaced by a more straightforward approach focusing on prediction. It consists in finding a direct relationship between the data and the forecast by a Bayesian evidential learning process (Scheidt *et al.* 2018). In Equation 12.52 (see Section 12.6), if we assume that the uncertainty of observed data ($p(\boldsymbol{y})$) is represented by a constant coefficient ($1/k$), the conditional probability $p(\boldsymbol{y}|\boldsymbol{b})$ of observing data $\boldsymbol{y}$ for a given set of parameter values $\boldsymbol{b}$ (also named likelihood function $L(\boldsymbol{y}|\boldsymbol{b})$) is equal to the product of $p(\boldsymbol{b})$ and $p(\boldsymbol{b}|\boldsymbol{y})$ (i.e., the *prior probability distribution* of the model parameter values multiplying the *posterior probability distribution* of the model parameter values expressing the conditional probability of obtaining a set of parameters for a given set of observed data):

$$p(\boldsymbol{b}|\boldsymbol{y}) = k\,p(\boldsymbol{b})\,p(\boldsymbol{y}|\boldsymbol{b}) = k\,p(\boldsymbol{b})\,L(\boldsymbol{y}|\boldsymbol{b}) \tag{12.58}$$

Here, PFA reformulates the Bayesian problem as follows:

$$p(\boldsymbol{h}|\boldsymbol{y}) = k\,p(\boldsymbol{h})\,L(\boldsymbol{h}|\boldsymbol{y}) \tag{12.59}$$

where $p(\boldsymbol{h}|\boldsymbol{y})$ is the *posterior distribution probability* of obtaining the prediction results $\boldsymbol{h}$ for a given set of observed data $\boldsymbol{y}$, $p(\boldsymbol{h})$ is the *prior distribution of probability* of the prediction results, and $L(\boldsymbol{h}|\boldsymbol{y})$ is the likelihood function measuring the fit between the observed $\boldsymbol{y}$ and calculated $\boldsymbol{h}$ data. Indeed, the whole difficulty lies in

- Avoid ratios higher than 1/10 for the cell dimensions, as it would induce highly contrasted coefficients in the equations (see Equation 13.18) producing bad numerical conditions (roundoff errors) for solving the whole system of n equations.
- If possible, boundaries with a prescribed head should preferably correspond to nodes (central points of the cells), while boundaries with a prescribed flux should be better chosen corresponding to sides of the cells (where the flux condition is calculated).

Transient groundwater flow

Keeping the same simplifying assumptions in the 2D groundwater flow equation, but introducing a second member for describing the transient conditions, another way to write Equation 4.90 is:

$$T\left(\frac{\partial^2 h}{\partial x^2}+\frac{\partial^2 h}{\partial y^2}\right)+q''=S\frac{\partial h}{\partial t} \tag{13.23}$$

with T and S assumed constant in the modeled domain (homogeneity and isotropy), q'' is the water flow rate per unit surface of the geological medium that is withdrawn ($q''<0$) or injected ($q''>0$) (see Section 4.11). Let's also assume that the spatial discretization corresponds to a uniform grid with square cells ($\Delta x=\Delta y=\Delta m$). The time derivative is replaced by a finite difference:

$$\frac{\partial h}{\partial t}\cong\frac{h(t+\Delta t)-h(t)}{\Delta t} \tag{13.24}$$

where Δt is the time step. A time step is the result of the time discretization. It is the subdivision of the time line in short periods during which the stress factors on the modeled system remain constant. A smaller time step provides a better estimate of the time derivative. The approximation error caused by the time discretization is directly proportional to the time step size (i.e., the time discretization error is of the first-order). The solution of the problem is computed for each time step and most often results are produced as model output at the end of each time step. In fact, if a new stress factor is started at the beginning of a considered time step, the variable of the system (e.g., piezometric head) evolves during the whole duration of the time step. One can physically observe that this evolution must be faster at the beginning of the time step than at the end (Figure 13.6).

Using the results of Equation 13.15 for approximating the spatial derivatives, and results of Equation 13.24 for the time derivative, Equation 13.23 for the cell i, j is now approximated by:

$$\frac{T}{(\Delta m)^2}(h_{i+1j}+h_{i-1j}+h_{ij+1}+h_{ij-1}-4h_{ij})+Q_{ij}=S\frac{h_{ij}(t+\Delta t)-h_{ij}(t)}{\Delta t} \tag{13.25}$$

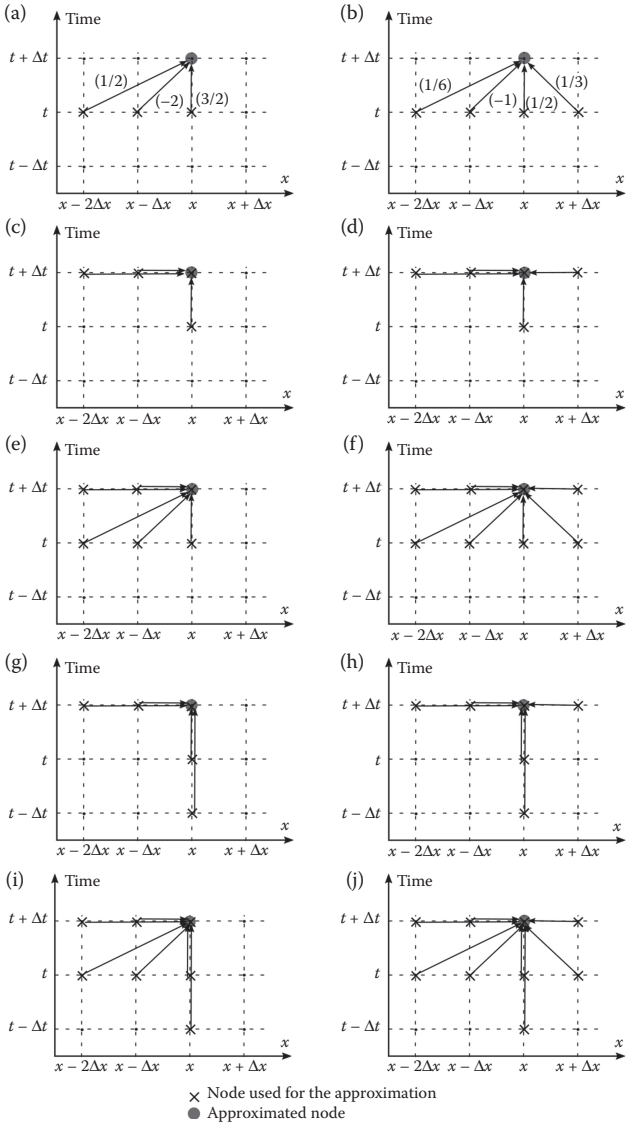

Figure 13.12 Schematic spatial and temporal view on the nodal contributions to the approximated $C(x,t + \Delta t)$ for a second-order (left) and a third-order spatial weighting (right) combined with different time integration schemes (explicit, implicit $\theta = 1$, Crank-Nicolson $\theta = 0.5$, first-order BDF implicit $\theta = 1$, **and third order partially explicit θ = 1/3)**. The following cases are shown: (a) second-order spatial upstream and explicit ($\theta = 0$), (b) third-order spa-tial upstream and explicit ($\theta = 0$), (c) second-order spatial upstream and implicit ($\theta = 1$), (d) third-order spatial upstream and implicit ($\theta = 1$), (e) second-order spatial upstream and Crank-Nicolson ($\theta = 1/2$), (f) third-order spatial upstream and Crank-Nicolson ($\theta = 1/2$), (g) second-order spatial upstream and first-order BDF implicit ($\theta = 1$), (h) third-order spatial upstream and first-order BDF implicit ($\theta = 1$), (i) second-order spatial upstream and third-order partially explicit ($\theta = 1/3$)), (j) third-order spatial upstream and third-order partially explicit ($\theta = (1/3)$).